LETTER

doi:10.1038/nature13589

CRISPR–mediated direct mutation of cancer genes in the mouse liver

Wen Xue[1]*, Sidi Chen[1]*, Hao Yin[1]*, Tuomas Tammela[1], Thales Papagiannakopoulos[1], Nikhil S. Joshi[1], Wenxin Cai[1], Gillian Yang[1], Roderick Bronson[2], Denise G. Crowley[1], Feng Zhang[3], Daniel G. Anderson[1,4,5,6], Phillip A. Sharp[1,7] & Tyler Jacks [1,7,8]

The study of cancer genes in mouse models has traditionally relied on genetically-engineered strains made via transgenesis or gene targeting in embryonic stem cells[1]. Here we describe a new method of cancer model generation using the CRISPR/Cas (clustered regularly interspaced short palindromic repeats/CRISPR-associated proteins) system *in vivo* in wild-type mice. We used hydrodynamic injection to deliver a CRISPR plasmid DNA expressing Cas9 and single guide RNAs (sgRNAs)[2–4] to the liver that directly target the tumour suppressor genes *Pten* (ref. 5) and *p53* (also known as *TP53* and *Trp53*) (ref. 6), alone and in combination. CRISPR-mediated *Pten* mutation led to elevated Akt phosphorylation and lipid accumulation in hepatocytes, phenocopying the effects of deletion of the gene using Cre–*LoxP* technology[7,8]. Simultaneous targeting of *Pten* and *p53* induced liver tumours that mimicked those caused by Cre–*loxP*-mediated deletion of *Pten* and *p53*. DNA sequencing of liver and tumour tissue revealed insertion or deletion mutations of the tumour suppressor genes, including bi-allelic mutations of both *Pten* and *p53* in tumours. Furthermore, co-injection of Cas9 plasmids harbouring sgRNAs targeting the β-catenin gene and a single-stranded DNA oligonucleotide donor carrying activating point mutations led to the generation of hepatocytes with nuclear localization of β-catenin. This study demonstrates the feasibility of direct mutation of tumour suppressor genes and oncogenes in the liver using the CRISPR/Cas system, which presents a new avenue for rapid development of liver cancer models and functional genomics.

The prokaryotic type II CRISPR/Cas genome editing tools have been successfully applied in many organisms, including mouse and human cells[2,4,9–11]. The system offers sequence-specific direct editing of DNA; therefore, unlike RNA-interference-based approaches[12], this method can achieve complete loss-of-function of the encoded protein. In rodent and primate embryonic stem cells or zygotes, CRISPR has been applied to efficiently generate mutant alleles or reporter genes[13–19]. Our groups have previously shown that *in vivo* delivery of CRISPR can repair a disease gene in mouse liver[20]. However, generation of somatic cancer mutations in adult animals using CRISPR has not, to our knowledge, been reported.

To investigate the potential of the CRISPR system to directly induce loss-of-function mutations *in vivo*, we chose to target the tumour suppressor gene *Pten*, which is a negative regulator of the phosphatidylinositol-3-kinase (PI3K)/Akt pathway[5]. Mutation and genomic loss of *Pten* has been identified in many types of human cancer[5] and liver-specific knockout of *Pten* in mice induces lipid accumulation and late-onset liver cancer[7,8]. We cloned a pX330 vector[9] co-expressing an sgRNA targeting *Pten* (Pten target sequence 1 in Supplementary Table 1, termed sgPten) and Cas9. We first showed that sgPten could induce *Pten* mutations in mouse 3T3 cells following transfection (Extended Data Fig. 1 and Supplementary Table 5). To deliver CRISPR to the liver in adult mice, we employed hydrodynamic tail-vein injection (Fig. 1a), which can deliver DNA to ~20% of hepatocytes for transient expression[21]. As shown in Fig. 1b, hydrodynamic injection of a luciferase plasmid DNA resulted in liver-specific expression of luciferase in mice. We next injected a cohort of FVB mice (an inbred wild-type mouse strain) with sgPten and an equal number of mice with a pX330 plasmid encoding an sgRNA targeting GFP (sgGFP) as a control. In parallel, we genetically deleted *Pten* in the liver of Pten-floxed mice[8] (*Pten*$^{fl/fl}$) via tail-vein injection of adenovirus expressing the Cre recombinase (adeno-Cre). Two weeks later, immunohistochemical (IHC) staining of liver sections from five of the sgPten-treated mice using a Pten-specific antibody revealed 3.3 ± 0.5% hepatocytes with negative Pten staining, surrounded by Pten-positive cells (Fig. 1c, d and Extended Data Fig. 2a–c). Importantly, the liver is composed of a mixture of diploid and polyploid hepatocytes, and we cannot determine the ploidy of the Pten-deficient cells. Thus, they may be a mixture of cells with two or more mutated *Pten* alleles. A lower percentage (0.4 ± 0.1%) of hepatocytes showed intermediate Pten staining (Fig. 1d and Extended Data Fig. 2c), potentially indicating heterozygous *Pten* mutation in diploid cells or incomplete mutation in polyploid cells. Coincident with negative Pten staining, we detected elevated staining of phospho-Akt (pAkt), a biomarker of the PI3K pathway activity, in sgPten-treated ($n = 5$) and adeno-Cre-injected *Pten*$^{fl/fl}$ mice ($n = 5$) (Fig. 1c bottom panel and Extended Data Fig. 2d). Histological analysis and Oil Red O staining at two months showed hepatocytes with lipid accumulation in sgPten-treated FVB mice ($n = 5$) and adeno-Cre-treated *Pten*$^{fl/fl}$ mice (Extended Data Fig. 3), which is a known phenotype associated with *Pten* mutation in the liver[7,8]. These data indicate that *in vivo* CRISPR-mediated genome editing was able to generate Pten-negative cells in the liver, mimicking liver-specific conditional deletion of *Pten* in mice.

To confirm that loss of Pten staining and function occurred due to CRISPR-mediated mutation of *Pten*, we performed deep sequencing on the captured targeted region of *Pten* locus of total liver genomic DNA. Sequencing revealed that 2.6 ± 1.4% of the sequencing reads had insertion or deletion mutations (indels) at the *Pten* locus in sgPten-treated mice ($n = 5$) compared to 0.5 ± 0.1% in sgGFP-treated mice ($n = 3$, $P = 0.02$) (Fig. 1e). In the sgPten-treated livers, most of the sequence variants were predicted to cause frameshift mutations as inferred from insertion length and/or phase (Fig. 1f, g and Extended Data Fig. 4). For example, we observed frequent occurrence of 1-nucleotide or 2-nucleotide indels, which would lead to disruption of the *Pten* reading frame (Fig. 1f–h and Supplementary Table 4). These indels clustered at the predicted sgPten-induced Cas9 cutting site (Fig. 1h and Extended Data Fig. 4a), whereas the indels detected in sgGFP samples distribute randomly at low frequency, probably due to background PCR errors or sequencing errors (Extended Data Fig. 4b). Notably, in five independent mice, the frequency of Pten loss scored by IHC (including both full and partial loss

[1]David H. Koch Institute for Integrative Cancer Research, Massachusetts Institute of Technology, Cambridge, Massachusetts 02142, USA. [2]Tufts University and Harvard Medical School, Boston, Massachusetts 02115, USA. [3]Broad Institute of Massachusetts Institute of Technology and Harvard, Cambridge, Massachusetts 02142, USA. [4]Department of Chemical Engineering, Massachusetts Institute of Technology, Cambridge, Massachusetts 02142, USA. [5]Harvard-MIT Division of Health Sciences & Technology, Cambridge, Massachusetts 02139, USA. [6]Institute for Medical Engineering and Science, Massachusetts Institute of Technology, Cambridge, Massachusetts 02142, USA. [7]Department of Biology, Massachusetts Institute of Technology, Cambridge, Massachusetts 02142, USA. [8]Howard Hughes Medical Institute, Massachusetts Institute of Technology, Cambridge, Massachusetts 02139, USA.
* These authors contributed equally to this work.

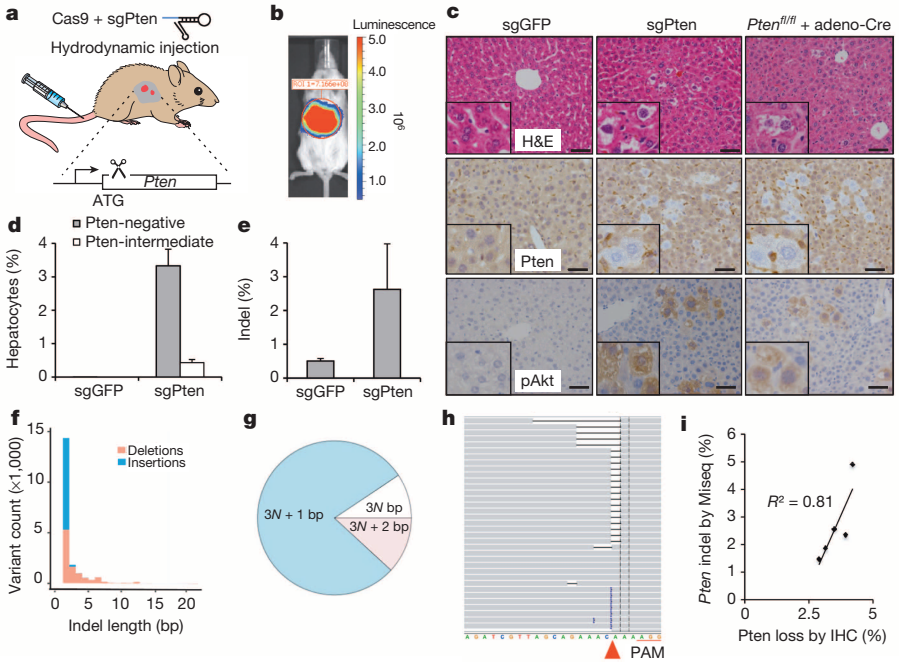

Figure 1 | Hydrodynamic injection of CRISPR deletes *Pten* in a subset of hepatocytes in mice. **a**, pX330 plasmids expressing Cas9 and sgRNA targeting *Pten* (sgPten) were hydrodynamically injected into wild-type FVB mice to transiently express the CRISPR components in hepatocytes. A cartoon of sgRNA is shown in the top right of the panel. **b**, Bioluminescence imaging of mice hydrodynamically injected with a luciferase plasmid shows liver-specific luciferase expression ($n = 3$). **c**, Representative haematoxylin and eosin (H&E) and IHC staining of FVB mice injected with sgGFP (as a control) or sgPten, and *Pten*$^{fl/fl}$ mice injected with adeno-Cre for 2 weeks. Note the hepatocytes with clear cytoplasm on H&E sections, indicating lipid accumulation. Scale bars are 50 μm. The insets are high-magnification views (×400). **d**, Percentage of hepatocytes with negative or intermediate Pten staining. Error bars are standard deviation (s.d.) ($n = 5$ mice). **e**, *Pten* indel frequency in the total liver genomic DNA. Error bars are s.d. ($n = 3$ mice for sgGFP and $n = 5$ mice for sgPten). **f**–**h**, Representative *Pten* indels in sgPten-treated mice. **f**, Distribution of indel length. **g**, Distribution of indel frame phase calculated as the length of indels modulus 3. For example, 1-, 4- and 7-base-pair indels are $3N+1$, 2-, 5- and 8-base-pair indels are $3N+2$ and 3-, 6- and 9-base-pair indels are $3N$. The pie chart shows the percentage of each class of indel types. **h**, Representative views of *Pten* indels in sgPten-treated mice using the Integrative Genomics Viewer. Black or purple bars indicate deletions or insertions, respectively. Arrowhead denotes predicted Cas9 cutting site. A full list of indels can be found in Supplementary Table 4. PAM, protospacer adjacent motif. **i**, Correlation between Pten loss determined by IHC and deep sequencing. Each dot is an individual mouse treated with sgPten.

of signal) strongly correlated with the frequency of *Pten* indels (Fig. 1i, $R^2 = 0.81$). These data indicate that for most cells, expression of the sgPten vector results in complete mutation of all *Pten* alleles present in the cell. Because non-parenchymal cells in the liver generally do not take up DNA following hydrodynamic injection, it is not surprising that the indel frequency in liver genomic DNA and the frequency of Pten-negative hepatocytes are not strictly equal.

To assess the long-term phenotype following sgPten treatment, we harvested livers from three sgPten-treated mice at four months. As shown in Fig. 2a, these livers exhibited regions of hepatocytes with prominent lipid accumulation, loss of Pten and increased pAkt staining, which phenocopies *Pten*-knockout mice[7,8]. To address whether sgPten induces p53 in hepatocytes, we performed p53 IHC on sgPten-treated liver sections at 14 days and 4 months. sgPten liver sections did not stain positively for p53, despite elevated pAkt (Fig. 2a and Extended Data Fig. 5), suggesting that Pten loss does not activate the p53 pathway in the liver at these time points. Given the long tumour latency of liver tumours in *Pten*-knockout mice (44–74 weeks)[7], we did not observe liver tumours in sgPten-treated mice at time points up to 4 months.

Recent studies identified that Cas9 can tolerate mismatches between sgRNA and genomic DNA depending on the sgRNA sequence and the position of the mismatches[9,22]. To characterize potential off-target effects of sgPten in the liver, we identified top-ranking sgPten off-target genomic sites in the mouse genome (Extended Data Fig. 6a) using a published prediction tool[9]. We amplified the *Pten* locus and the top four potential off-target sites from sgGFP- and sgPten-treated livers and measured CRISPR editing using the Surveyor assay[2]. In the sgPten-treated livers, the assay revealed 2.3 ± 0.4% ($n = 2$) indels at the *Pten* locus. In contrast, we did not detect Surveyor nuclease cutting at the assayed off-target sites (Extended Data Fig. 6b), indicating that the frequency of off-target editing is below the limit of detection of this assay. Deep sequencing of an sgPten-treated liver sample revealed that the indel frequency within 10-nucleotide regions around the top three predicted cutting sites was <0.1% (Supplementary Table 6).

We next tested a nickase version of Cas9, Cas9(D10A), which only makes single-strand DNA (ssDNA) breaks and was reported to have further reduced levels of off-target effects[23,24]. We designed a pair of Pten sgRNAs (Fig. 2b) predicted to generate off-set ssDNA breaks[24]. The Cas9^{D10A} plasmid and the two PCR products containing a U6 promoter driving expression of off-set Pten sgRNAs (termed sgPten.2/3) were introduced into FVB mice ($n = 5$) by hydrodynamic injection. U6-sgGFP PCR DNA served as a control ($n = 5$). By deep sequencing of the liver genomic DNA isolated from two mice at two weeks post-injection, we observed 2.7 ± 0.1% indels at the *Pten* locus in sgPten.2/3-treated mice compared to 0.2 ± 0.2% in sgGFP-treated mice ($n = 2$) (Fig. 2c, d and Extended Data Fig. 4c and Supplementary Table 4). Pten-negative cells were observed in the sgPten.2/3 livers (2.8 ± 0.4%) but not in sgGFP controls (0.0 ± 0.0%) by IHC staining (Fig. 2e) ($n = 5$).

To test whether CRISPR-mediated mutation can target other tumour suppressor genes *in vivo*, we designed constructs to mutate *p53* (also known as *TP53* and *Trp53*), which is the most frequently mutated tumour suppressor gene in human cancer[6]. Exome-sequencing studies have identified frequent mutations of *p53* and *PTEN* in human cholangiocarcinoma[25]. An sgRNA construct targeting *p53* was cloned into the pX330 plasmid (termed sgp53)[26]. Transfection of sgp53 into 3T3 cells led to frequent *p53* indels, as measured by deep sequencing (Extended

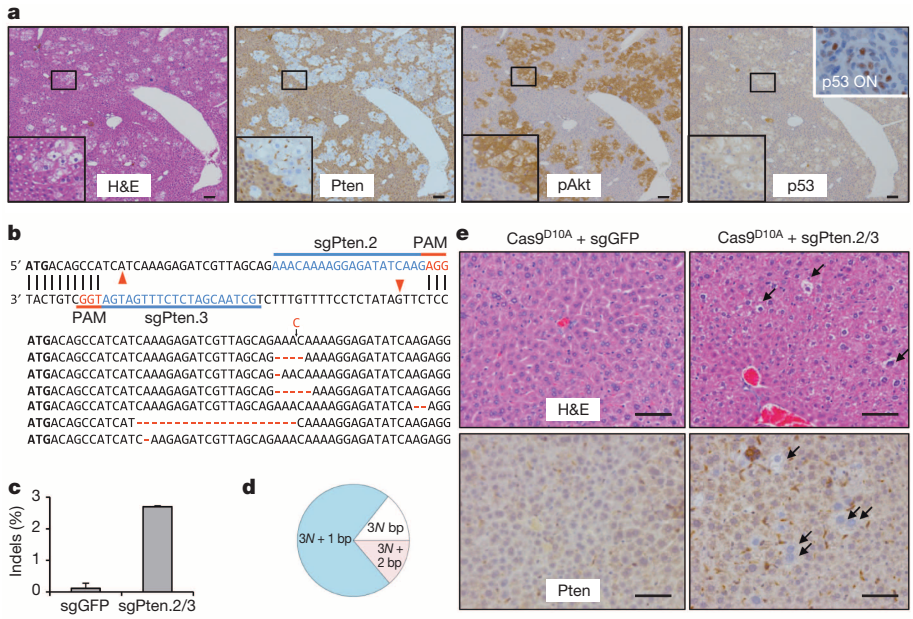

Figure 2 | Long-term effects of sgPten in the liver and off-set CRISPR double nickase strategy. **a**, IHC on serial liver sections from sgPten-treated mice at 4 months post-injection. Scale bars are 100 μm. $n = 3$ mice. The lower-left insets are high-magnification views (×120). The 'p53 ON' inset is a p53-restored liver tumour as a positive control[30]. **b**, FVB mice were injected with $Cas9^{D10A}$ plus sgGFP (as a control) or plus a pair of off-set sgRNAs targeting Pten (sgPten.2 and sgPten.3) to introduce double nicking. Red arrowheads denote predicted $Cas9^{D10A}$ cutting sites. Total liver genomic DNA was analysed by deep sequencing for *Pten* indels. Representative sequences are shown. Red lines denote deletions, the black arrow denotes an insertion. **c**, Frequency of *Pten* indels ($n = 2$ mice). Error bars are s.d. **d**, Frame phase of *Pten* indels calculated as the length of indels modulus 3. **e**, H&E and Pten IHC staining of liver sections. Arrows denote cells showing negative Pten staining or lipid accumulation. $n = 5$ mice. Scale bar is 50 μm.

Data Fig. 7 and Supplementary Table 5). We next injected a cohort of FVB mice with sgp53 alone. These mice did not exhibit liver tumours at three months post-injection (Extended Data Fig. 8a), which is consistent with previous studies showing that liver-specific *p53*-knockout mice develop liver tumours only after 14 months[27]. We also performed deep sequencing of sgp53-treated livers at 14 days and detected 6.0 ± 0.1% indels at the *p53* locus (Extended Data Fig. 8b and Supplementary Table 4), demonstrating that sgp53 can directly generate mutations in *p53* in the mouse liver.

In an effort to mutate two tumour suppressor genes simultaneously, we co-injected sgPten and sgp53 into FVB mice (Fig. 3a). As shown in Fig. 3b and Extended Data Fig. 9, indels were observed in total liver DNA isolated from two animals, at frequencies of 4.0 ± 0.1% for *Pten* and 6.4 ± 0.1% for *p53*, enriched at the predicted cutting sites. At 3 months post-injection, all 5 mice co-injected with sgPten and sgp53 developed liver tumours with bile duct differentiation features (Fig. 3c), whereas none of sgGFP-injected mice ($n = 5$) developed tumours. The tumours were positive for cytokeratin 19, a marker of bilinear lineage cells[27] (Fig. 3c). $Pten^{fl/fl}$;$p53^{fl/fl}$ conditional knockout mice ($n = 5$) injected with adeno-Cre also developed liver tumours of similar histology at 3 months (Fig. 3c). When injected alone, neither sgPten nor sgp53 caused any detectable tumours at this time point. Sequencing of the sgPten- plus sgp53-induced liver tumours and tumour-derived cell lines ($n = 5$ tumours analysed) showed bi-allelic mutations of both genes (Fig. 3d and Supplementary Table 7). These results demonstrate that CRISPR-mediated mutation of *Pten* and *p53* can induce liver tumour development, supporting the use of multiplexed CRISPR editing of cancer genes, at least in this tissue.

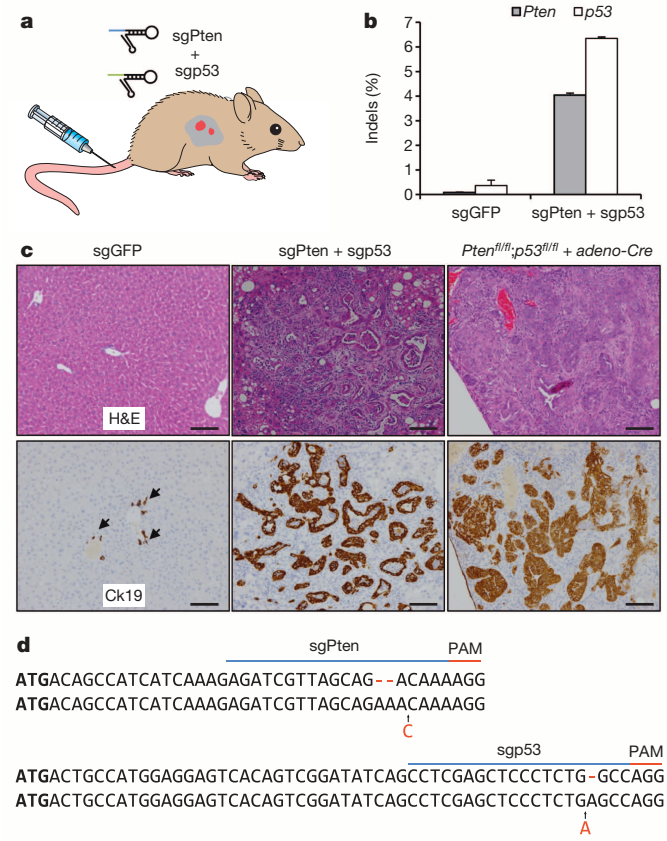

Figure 3 | Multiplexed CRISPR targeting *Pten* and *p53* induces tumour formation in murine liver. **a**, pX330 plasmids expressing sgPten and sgp53 were hydrodynamically injected into FVB mice. **b**, Frequency of *Pten* and *p53* indels quantified by Illumina MiSeq ($n = 2$ mice) at 14 days post-injection. Error bars are s.d. **c**, Representative H&E and IHC staining of FVB mice injected with sgGFP (as a control) or sgPten + sgp53, and $Pten^{fl/fl}$;$p53^{fl/fl}$ mice injected with adeno-Cre. Arrows indicate cytokeratin-19-positive bile duct cells in sgGFP mice. Scale bars are 100 μm. $n = 5$ mice. **d**, Representative sequences of *Pten* and *p53* loci in sgPten + sgp53 induced liver tumours ($n = 5$ tumours). Red lines denote deletions, black arrows denote insertions.

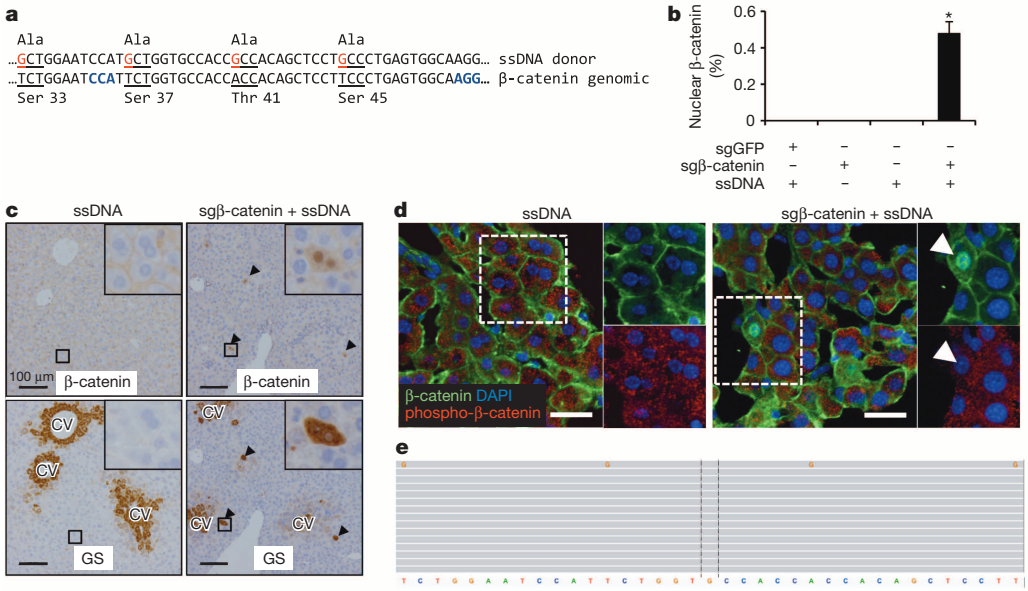

Figure 4 | CRISPR introduces β-catenin mutations in the liver. **a**, FVB mice were co-injected with two sgRNAs targeting the β-catenin gene *Ctnnb1* (sgβ-catenin) and a 200-nucleotide ssDNA oligonucleotide containing four alanine point mutations (red) which abolish the phosphorylation of serine and threonine sites of β-catenin. Codons are underlined. Protospacer adjacent motif (PAM) sequences are marked in blue. **b**, Quantification of hepatocytes with nuclear β-catenin IHC staining at day 7. Mice were injected with indicated combination. sgGFP serves as a control sgRNA. $n = 5$ mice, $^*P < 0.05$. Error bars are s.d. **c**, IHC on serial liver sections. Glutamine synthetase (GS) is normally expressed surrounding the central veins (left). Arrowheads indicate overlap of β-catenin and GS staining outside the central vein (CV) region (right). Scale bars are 100 μm. The insets are high-magnification views (×400). **d**, Single confocal sections show nuclear β-catenin and loss of cytoplasmic phospho-β-catenin in the cell indicated by an arrow. Scale bars are 100 μm. The insets are ×400 magnification views. **e**, Representative *Ctnnb1* deep sequencing reads in sgβ-catenin + ssDNA-treated mice. Each grey bar represents a sequencing read. *Ctnnb1* reference sequence is shown at the bottom. Reads matching the reference sequence are in grey. Variant bases are in colours (G in orange). $n = 2$ mice.

To determine whether CRISPR can be used to directly introduce gain-of-function mutations, we targeted the *Ctnnb1* gene, which encodes β-catenin, a transcription factor in the Wnt signalling pathway that is frequently mutated in liver cancer[28]. Phosphorylation of four serine/threonine residues leads to degradation of β-catenin (Fig. 4a)[28]. We co-injected FVB mice with two pX330 plasmids carrying sgRNAs targeting *Ctnnb1* (termed sgβ-catenin) and a 200-nucleotide ssDNA oligonucleotide containing four point mutations that cause serine/threonine to be replaced with alanine (Fig. 4a), which together have been shown to abolish phosphorylation and cause stabilization and nuclear localization of β-catenin (ref. 28). In mice injected with either sgβ-catenin or ssDNA alone ($n = 5$), β-catenin was localized only at cell junctions as shown by IHC (Fig. 4b, c). In contrast, in five mice injected with sgβ-catenin and ssDNA, we observed that ~0.5% of hepatocytes exhibited nuclear β-catenin at 7 days post-injection (Fig. 4b, c). Moreover, accumulation of β-catenin was associated with increased levels of glutamine synthetase, a β-catenin target gene[29] in the liver (Fig. 4c and Extended Data Fig. 10a) and reduced phospho-β-catenin (Fig. 4d). In addition, we subjected the liver DNA from two mice treated with this combination to deep sequencing. The data confirm that a small but detectable percentage of sequencing reads contained the four 'G' point mutations present in the ssDNA (Fig. 4e and Extended Data Fig. 10b). Single-guide β-catenin also generated indels clustered at the predicted Cas9 cutting sites (Supplementary Table 8). These data demonstrate that CRISPR system can be used to directly induce gain-of-function mutation or other substitutions via homologous recombination *in vivo*[20].

Our data illustrate the potential to directly disrupt tumour suppressor genes and generate point mutations in oncogenes in adult mouse liver using the CRISPR/Cas system. This method bypasses the need to engineer embryonic stem cells and to breed multiple mutant animals together to generate compound mutants. This approach generated compound *Pten* and *p53* indels at low frequency but was sufficient to induce multifocal tumours. We anticipate that this method will allow for more rapid testing of any single genes or gene combinations that are suspected of being capable of initiating tumour formation in the liver. Given the number of candidate cancer genes being discovered through next generation sequencing efforts, simplified methods of testing the oncogenic properties of candidates *in vivo* are critical. To increase the sensitivity of the assay, one could perform the CRISPR/Cas9-mediated mutagenesis on a 'sensitized' background carrying constitutive or conditional mutations in a tumour suppressor gene such as *p53*. More efficient delivery techniques, such as adenovirus or adeno-associated virus (F.A. Ran *et al.*, submitted), more potent sgRNAs, and longer homologous recombination templates might also improve the overall efficiency of this method and expand the range of tissue that could be targeted. Consistent with recent studies showing that long-term Cas9/sgRNA expression is not toxic in cells[26], hydrodynamic injection of Cas9/sgGFP in mice was well tolerated and did not trigger weight loss in mice[20]. However, further studies are required to fully evaluate the side effects of the CRISPR system in mice and other organisms. This study underscores the power of the CRISPR/Cas9 system for rapid genome editing and the development of novel cancer models in the mouse.

Online Content Methods, along with any additional Extended Data display items and Source Data, are available in the online version of the paper; references unique to these sections appear only in the online paper.

Received 18 February; accepted 17 June 2014.
Published online 6 August 2014.

1. Van Dyke, T. & Jacks, T. Cancer modeling in the modern era: progress and challenges. *Cell* **108,** 135–144 (2002).
2. Cong, L. *et al.* Multiplex genome engineering using CRISPR/Cas systems. *Science* **339,** 819–823 (2013).
3. Jinek, M. *et al.* A programmable dual-RNA-guided DNA endonuclease in adaptive bacterial immunity. *Science* **337,** 816–821 (2012).
4. Mali, P. *et al.* RNA-guided human genome engineering via Cas9. *Science* **339,** 823–826 (2013).
5. Song, M. S., Salmena, L. & Pandolfi, P. P. The functions and regulation of the *PTEN* tumour suppressor. *Nature Rev. Mol. Cell Biol.* **13,** 283–296 (2013).
6. Feldser, D. M. *et al.* Stage-specific sensitivity to *p53* restoration during lung cancer progression. *Nature* **468,** 572–575 (2010).

7. Horie, Y. *et al.* Hepatocyte-specific Pten deficiency results in steatohepatitis and hepatocellular carcinomas. *J. Clin. Invest.* **113,** 1774–1783 (2004).
8. Stiles, B. *et al.* Liver-specific deletion of negative regulator *Pten* results in fatty liver and insulin hypersensitivity. *Proc. Natl Acad. Sci. USA* **101,** 2082–2087 (2004).
9. Hsu, P. D. *et al.* DNA targeting specificity of RNA-guided Cas9 nucleases. *Nature Biotechnol.* **31,** 827–832 (2013).
10. Mali, P., Esvelt, K. M. & Church, G. M. Cas9 as a versatile tool for engineering biology. *Nature Methods* **10,** 957–963 (2013).
11. Sander, J. D. & Joung, J. K. CRISPR-Cas systems for editing, regulating and targeting genomes. *Nature Biotechnol.* **32,** 347–355 (2014).
12. Fellmann, C. & Lowe, S. W. Stable RNA interference rules for silencing. *Nature Cell Biol.* **16,** 10–18 (2013).
13. Wang, H. *et al.* One-step generation of mice carrying mutations in multiple genes by CRISPR/Cas-mediated genome engineering. *Cell* **153,** 910–918 (2013).
14. Yang, H. *et al.* One-step generation of mice carrying reporter and conditional alleles by CRISPR/Cas-mediated genome engineering. *Cell* **154,** 1370–1379 (2013).
15. Li, W., Teng, F., Li, T. & Zhou, Q. Simultaneous generation and germline transmission of multiple gene mutations in rat using CRISPR-Cas systems. *Nature Biotechnol.* **31,** 684–686 (2013).
16. Li, D. *et al.* Heritable gene targeting in the mouse and rat using a CRISPR-Cas system. *Nature Biotechnol.* **31,** 681–683 (2013).
17. Shen, B. *et al.* Generation of gene-modified mice via Cas9/RNA-mediated gene targeting. *Cell Res.* **23,** 720–723 (2013).
18. Wu, Y. *et al.* Correction of a genetic disease in mouse via use of CRISPR-Cas9. *Cell Stem Cell* **13,** 659–662 (2013).
19. Niu, Y. *et al.* Generation of gene-modified cynomolgus monkey via Cas9/RNA-mediated gene targeting in one-cell embryos. *Cell* **156,** 836–843 (2014).
20. Yin, H. *et al.* Genome editing with Cas9 in adult mice corrects a disease mutation and phenotype. *Nature Biotechnol.* **32,** 551–553 (2014).
21. Liu, F., Song, Y. & Liu, D. Hydrodynamics-based transfection in animals by systemic administration of plasmid DNA. *Gene Ther.* **6,** 1258–1266 (1999).
22. Fu, Y. *et al.* High-frequency off-target mutagenesis induced by CRISPR-Cas nucleases in human cells. *Nature Biotechnol.* **31,** 822–826 (2013).
23. Mali, P. *et al.* Cas9 transcriptional activators for target specificity screening and paired nickases for cooperative genome engineering. *Nature Biotechnol.* **31,** 833–838 (2013).
24. Ran, F. A. *et al.* Double nicking by RNA-guided CRISPR Cas9 for enhanced genome editing specificity. *Cell* **154,** 1380–1389 (2013).
25. Ong, C. K. *et al.* Exome sequencing of liver fluke-associated cholangiocarcinoma. *Nature Genet.* **44,** 690–693 (2012).
26. Malina, A. *et al.* Repurposing CRISPR/Cas9 for *in situ* functional assays. *Genes Dev.* **27,** 2602–2614 (2013).
27. Katz, S. F. *et al.* Disruption of Trp53 in livers of mice induces formation of carcinomas with bilineal differentiation. *Gastroenterology* **142,** 1229–1239 (2012).
28. Moon, R. T., Kohn, A. D., De Ferrari, G. V. & Kaykas, A. Wnt and β-catenin signalling: diseases and therapies. *Nature Rev. Genet.* **5,** 691–701 (2004).
29. Tward, A. D. *et al.* Distinct pathways of genomic progression to benign and malignant tumors of the liver. *Proc. Natl Acad. Sci. USA* **104,** 14771–14776 (2007).
30. Xue, W. *et al.* Senescence and tumour clearance is triggered by *p53* restoration in murine liver carcinomas. *Nature* **445,** 656–660 (2007).

Supplementary Information is available in the online version of the paper.

Acknowledgements We thank D. McFadden, N. Dimitrova, E. Snyder, A. Farago, M. Muzumdar, F. Sanchez-Rivera, J. Doench, L. Cong and S. Levine for discussions and for sharing reagents. We thank the Koch Institute Swanson Biotechnology Center (SBC) for technical support, specifically the Hope Babette Tang (1983) Histology Facility and K. Cormier. This work was supported by grants 2-PO1-CA42063, RO1-EB000244, RO1-CA115527 and RO1-CA132091 from the National Institutes of Health and supported in part by Cancer Center Support (core) grant P30-CA14051 from the National Cancer Institute. This work was supported, in part, by NIH Grant R01-CA133404 and Casimir-Lambert Fund to P.A.S. H.Y. is supported by 5-U54-CA151884-04 NIH Centers for Cancer Nanotechnology Excellence and the Harvard-MIT Center of Cancer Nanotechnology Excellence. S.C. is a Damon Runyon Fellow (DRG-2117-12). W.X. was supported by fellowships from the American Association for Cancer Research and the Leukemia Lymphoma Society and is currently supported by grant 1K99CA169512. T.J. is a Howard Hughes Medical Institute (HHMI) Investigator, the David H. Koch Professor of Biology, and a Daniel K. Ludwig Scholar.

Author Contributions W.X., S.C., H.Y. and T.J. designed the study. W.X., S.C., H.Y., T.T., W.C. and G.Y. performed experiments and analysed data. D.G.C. and R.B. performed histology and evaluations. T.P., N.S.J., F.Z. and D.A.G. provided reagents and conceptual advice. W.X., S.C., H.Y., P.A.S. and T.J. wrote the manuscript with comments from all authors.

Author Information Data generated during the work are deposited at NCBI BioProject under accession code PRJNA252101. Reprints and permissions information is available at www.nature.com/reprints. The authors declare no competing financial interests. Readers are welcome to comment on the online version of the paper. Correspondence and requests for materials should be addressed to T.J. (tjacks@mit.edu).

METHODS

CRISPR vectors. pX330 vector[9] was digested with BbsI and ligated with annealed oligonucleotides (Supplementary Table 1). An extra G is added for sgRNAs lacking a 5′ G for U6 transcriptional initiation. Cas9^{D10A} nickase vector was from addgene[4]. sgPten.2 and sgPten.3 were PCR amplified from empty pX330 plasmid using the U6 forward primer and sgRNA reverse ultramer oligonucleotides[9] (Supplementary Tables 2 and 3) and PCR purified.

Mice and hydrodynamic injection. All animal study protocols were approved by the MIT Animal Care and Use Committee. Cohorts of *Pten*$^{fl/fl}$ and *Pten*$^{fl/fl}$;*p53*$^{fl/fl}$ mice were infected with 1×10^8 (Fig. 1) or 1×10^9 (Fig. 3) plaque-forming units (PFU) of adeno-Cre (University of Iowa) in 100 μl PBS by intravenous injection. Vectors for hydrodynamic tail-vein injection were prepared using the EndoFree-Maxi Kit (Qiagen). For hydrodynamic liver injection, plasmid DNA suspended in 2 ml saline was injected via the tail vein in 5–7 s into 8-week-old female FVB/NJ mice (Jackson lab). No randomization or blinding was used. The amount of injected DNA was 60 μg for sgPten, 60 μg each for sgPten + sgp53, 40 μg Cas9^{D10A} + 2μg sg Pten2 PCR + 2 μg sgPten.3 PCR for off-set sgRNA study, and 30 μg sgβ-catenin.1, 30 μg sgβ-catenin.2 and 60 μg ssDNA for the β-catenin experiment. An equal amount of sgGFP was used as a control for each experiment. The *Pten*$^{fl/fl}$;*p53*$^{fl/fl}$ and sgPten + sgp53 mice were dosed with CCl_4 as in ref. 31.

Immunohistochemistry and immunofluorescence. Mice were killed by carbon dioxide asphyxiation. Livers were fixed in 4% formalin overnight, embedded in paraffin, sectioned at 4 μm and stained with hematoxylin and eosin (H&E) for pathology. Liver sections were de-waxed, rehydrated and stained using standard immunohistochemistry protocols[32]. The following antibodies were used: anti-Pten (Cell Signaling, 9559, 1:100), anti-pAkt S473 (Cell Signaling, 4060, 1:50), β-catenin (BD, 610154, 1:100), anti-p53 (CM5, 1:300), anti-glutamine synthetase (BD 610517, 1:200) and anti-cytokeratin 19 (Abcam, ab133496, 1:100). The number of hepatocytes was quantified from >3 low-magnification fields per mouse with 5 mice per group. Immunofluorescence was performed as previously described[32]. β-catenin (BD,610154) and phospho-β-catenin (Abcam, ab53050) antibodies were used. Slides were counterstained with 4,6-diamidino-2-phenylindole (DAPI). Images were obtained with a Nikon A1R laser scanning confocal microscope using a ×40 APO Fluor objective (NA 0.65).

Bioluminescence imaging. 5 μg luciferase plasmids were hydrodynamically injected into FVB mice. 24 h later, bioluminescence imaging (Xenogen) was performed as previously described[32].

Genomic DNA purification and Surveyor assay. Genomic DNA from liver or tumour tissue was purified from High Pure PCR Template Preparation Kit (Roche 11796828001). 3T3 cells were transiently transfected with pX330 and a GFP plasmid. Top 20% GFP$^+$ cells were sorted by FACS and genomic DNA was purified at 72 h post-transfection. Off-target sites were predicted using http://crispr.mit.edu/. For the Surveyor assay, PCR products (Supplementary Table 3) were gel purified and treated with Surveyor nuclease kit (Transgenomic). DNA was separated on 4–20% Novex TBE Gels (Life Technologies) and stained with ethidium bromide. Quantification of surveyor bands was as in ref. 9. For sequencing of liver tumours and matched tumour-derived cell lines, PCR products of the *Pten* and *p53* genomic regions were cloned using Zero Blunt TOPO PCR Cloning Kit (Life Technologies) and analysed by Sanger sequencing. One tumour from each animal was analysed.

Deep sequencing of CRISPR modified *Pten* and *p53* loci. The genomic region of *Pten* and *p53* was PCR amplified using Herculase II high-fidelity polymerase and gel purified. Libraries were made from 50 ng of the PCR products using the Nextera protocol and sequenced on Illumina MiSeq (150 base pair (bp) paired-end) and HiSeq2500 (100 bp paired-end, β-catenin samples) machines. Data were processed according to standard Illumina sequencing analysis procedures. Briefly, reads were mapped to the PCR amplicons as reference sequences using Burrows–Wheeler Aligner with custom scripts[33]. Insertions and deletions were crosschecked against reference using VarScan2. Indel phase was calculated as the length of insertions or deletions modulus 3. The rate of β-catenin donor integration was calculated as donor allele frequency. Indels at Pten G304 exist at the same frequency across all samples, thus possibly arise from PCR or sequencing errors, and were filtered out in final analysis. Two to five biological replicates were sequenced for *in vivo* liver samples. One DNA sample was sequenced for *Pten* and *p53* in 3T3 cells and for *Pten* off-target sites in sgPten-treated liver. To compare the editing efficiency at *Pten* off-target sites, the indel frequency within 10-nucleotide regions (20 nucleotides total) flanking *Pten* A124, OT1 G209, OT2 G451, OT3 G265 was calculated.

Statistics. *P* values were determined by Student's *t*-tests and ANOVA for all IHC quantifications.

31. Zender, L. *et al.* Identification and validation of oncogenes in liver cancer using an integrative oncogenomic approach. *Cell* **125,** 1253–1267 (2006).
32. Xue, W. *et al.* Response and resistance to NF-κB inhibitors in mouse models of lung adenocarcinoma. *Cancer Discov.* **1,** 236–247 (2011).
33. Chen, S. *et al.* Global microRNA depletion suppresses tumor angiogenesis. *Genes Dev.* **28,** 1054–1067 (2014).

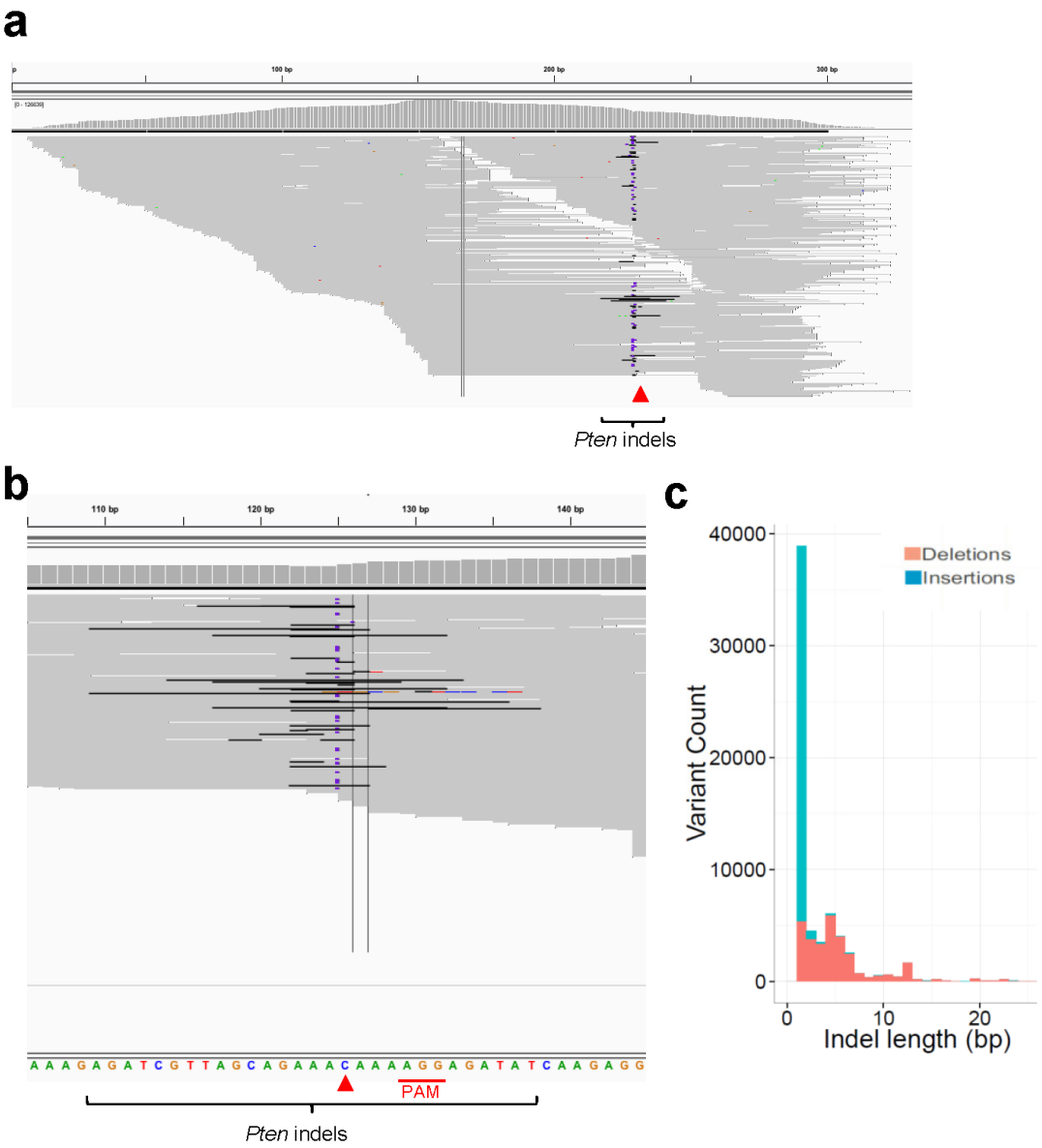

Extended Data Figure 1 | Representative *Pten* indels in sgPten-treated 3T3 cells. Mouse 3T3 cells were co-transfected with sgPten and a GFP plasmid. The highest 20% of GFP-positive cells were sorted to enrich for cells expressing sgPten. Deep sequencing of the *Pten* locus revealed 36.4% *Pten* indels in this context (Supplementary Table 5), presumably due to the more efficient delivery of sgPten via cell culture transfection and sorting. Red arrowheads denote predicted Cas9 cutting sites. Black or purple bars in grey sequencing reads indicate deletions or insertions, respectively. Other colours indicate SNPs. **a**, *Pten* PCR region. **b**, Zoom in view. $n = 1$ DNA sample. **c**, Distribution of *Pten* indel length.

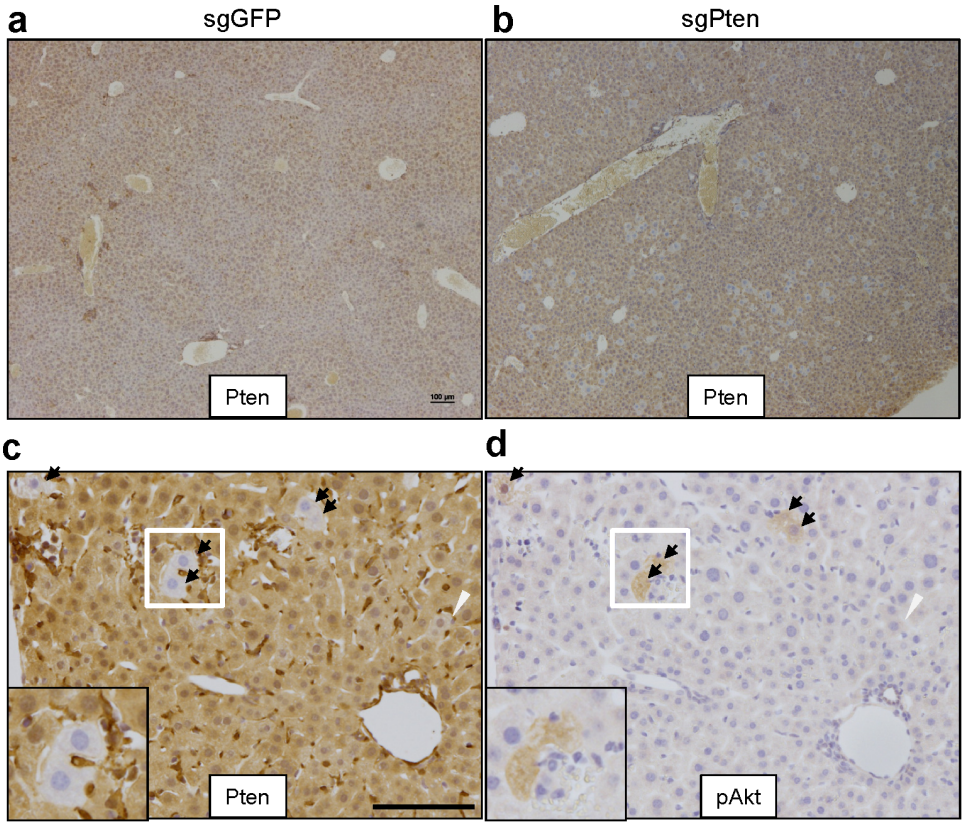

Extended Data Figure 2 | CRISPR generates Pten-negative hepatocytes *in vivo*. **a**, **b**, Low-magnification images of Pten IHC in sgGFP- (**a**) and sgPten-treated (**b**) mice. Scale bar is 100 μm. **c**, **d**, IHC on serial sections from sgPten-treated mice. Black arrows denote cells with negative Pten staining and positive pAkt staining. White arrowhead denotes cells with intermediate Pten staining, potentially indicating heterozygous Pten mutation or multi-nucleated hepatocytes with partial Pten loss. Insets show high-magnification IHC images. Scale bar is 100 μm. $n = 5$ mice. The frequency of Pten-deficient cells is probably a reflection of the transduction efficiency following hydrodynamic injection and the time required to achieve mutation. A recent study by our groups has shown that ~17% of hepatocytes were Flag–Cas9 positive as indicated by IHC 24 h after hydrodynamic injection, only 1.4% of cells on day 7, and less than 0.3% at one month[20]. Given that Cas9-mediated genome editing usually takes more than 48 h (ref. 2), the fraction of hepatocytes that productively express Cas9 and an sgRNA after hydrodynamic injection is estimated to be less than 17%.

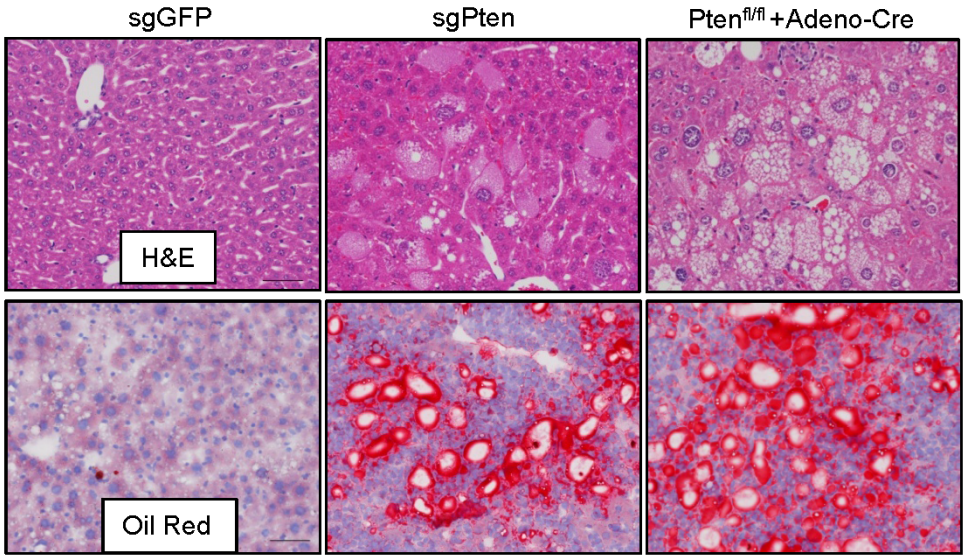

Extended Data Figure 3 | sgPten induces lipid accumulation in the liver. FVB mice were injected with sgGFP or sgPten ($n = 5$). 2 months later, liver sections were stained for Oil Red O, a marker for lipid accumulation. Scale bars are 50 μm.

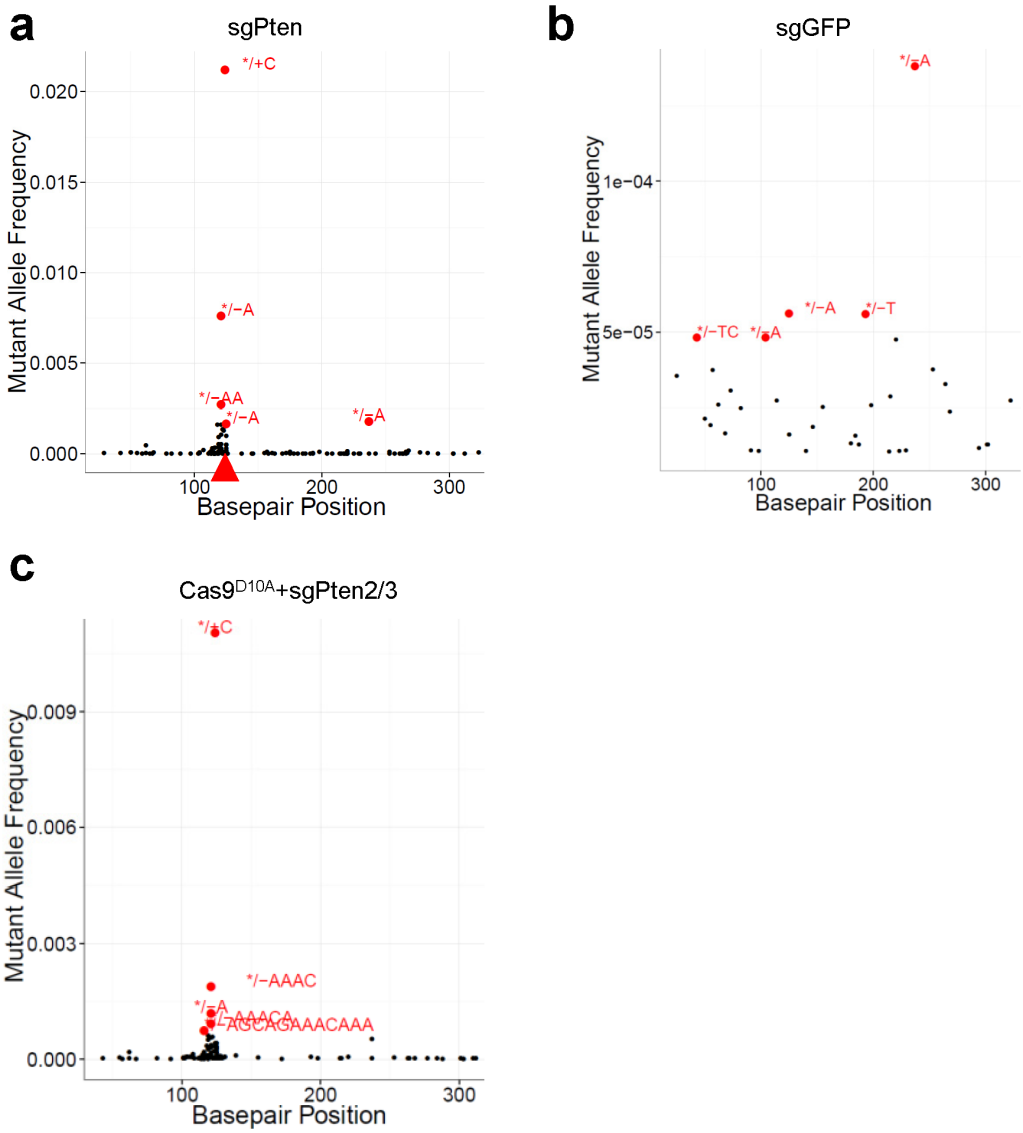

Extended Data Figure 4 | sgPten generated indels at the *Pten* locus in the liver. **a**, Representative indel frequency. Base pair position denotes position along the *Pten* reference sequence. **b**, Representative *Pten* indel frequency in sgGFP mice. Note the low mutant allele frequency compared to **a**. sgPten samples show indels peaking at the predicted Cas9 cutting site whereas sgGFP indels distribute randomly. **c**, Representative indel frequency in $Cas9^{D10A}$ + sgPten.2/3-treated mice. For all panels */+x denotes insertion of x nucleotides, */−x denotes deletion of x nucleotides.

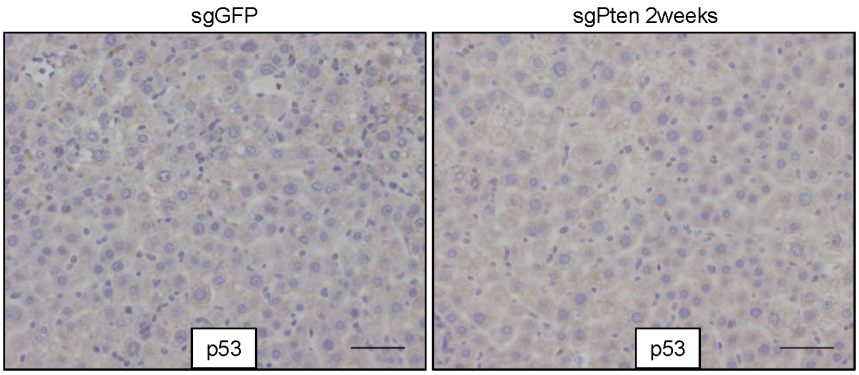

Extended Data Figure 5 | Pten deletion in the liver does not induce p53. Liver sections from sgGFP- or sgPten-treated mice at 2 weeks were stained for p53 IHC. $n = 3$ mice. Scale bars are 50 μm. Positive control from a p53-restoration tumour is shown in the inset of Fig. 2a (p53 ON)[30].

a

ID	Sequence (20nt+PAM)	score	mismatches	UCSC gene	locus
1	AGATGGTGACCAGAAACAAACAG	2.3	3MMs [5:8:10]		chr7:-56172579
2	AAATCATCAGCAGAAACAAACAG	1.5	3MMs [2:6:8]		chr5:-81530627
3	AGAGTGTTAGCAGAAACAATTGG	1.4	3MMs [4:5:20]		chr11:+22233525
4	GCATTGTTACCAGAAACAAACAG	1.3	4MMs [1:2:5:10]	NR_045386	chr18:+49962998
5	CAATGGTTAACAGAAACAAAAAG	1.3	4MMs [1:2:5:10]		chr13:+51519545
6	AGATTGTTAAAAGAAACAAATAG	1.3	3MMs [5:10:11]		chr1:+28342977
7	AAATGGTCACCAGAAACAAAAAG	1.3	4MMs [2:5:8:10]		chr16:+97448451
8	ATATGGTTAGCAGAAAAAAAAAG	1.3	3MMs [2:5:17]		chr2:-118247411
9	AGAAAGTTAGCAGAAACATATGG	1	3MMs [4:5:19]		chr1:+61494552
10	AGATTGGTGGCAGAAACAAACAG	1	3MMs [5:7:9]		chr3:+80611324
11	AGAGCACTAGCAGAAACAAAGGG	1	3MMs [4:6:7]		chr2:-114897270
12	AGATTGTTATCACAAACAAATGG	1	3MMs [5:10:13]		chr6:-74006099
13	AAATCATTAGAAGAAACAAAGAG	0.9	3MMs [2:6:11]		chr4:+71593592
14	TAATTGTTTGCAGAAACAAAAGG	0.9	4MMs [1:2:5:9]		chr10:-20775651
15	AGACAGATAACAGAAACAAATAG	0.9	4MMs [4:5:7:10]		chr12:-67842263
16	GAATCTTGAGCAGAAACAAATGG	0.8	4MMs [1:2:6:8]		chr3:-19546766
17	AAATTATCAGCAGAAACAAATGG	0.8	4MMs [2:5:6:8]		chr6:-31440319
18	AACTCCTAAGCAGAAACAAAAGG	0.8	4MMs [2:3:6:8]		chr3:+93150452
19	ATAATTTTAGCAGAAACAAATGG	0.8	4MMs [2:4:5:6]		chrX:+5661815
20	TGATCATAAACAGAAACAAATAG	0.8	4MMs [1:6:8:10]		chr9:+82430572
21	AAAAGGTTAGGAGAAACAAAAAG	0.8	4MMs [2:4:5:11]		chr5:-84250058
22	AGATGGCTAGCAGAAAAAAAAGG	0.8	3MMs [5:7:17]		chr10:+122331741
23	AGGAAATTAGCAGAAACAAAAAG	0.8	4MMs [3:4:5:6]		chr16:+76862019
24	AGACTGTTGACAGAAACAAAAAG	0.8	4MMs [4:5:9:10]		chr9:-4831483
25	AGGTGTTTATCAGAAACAAAAGG	0.8	4MMs [3:5:6:10]		chr18:-21529555
26	AGAATTTTAACAGAAACAAACAG	0.8	4MMs [4:5:6:10]		chr17:+82812663
27	AGAAATTTACCAGAAACAAAGAG	0.8	4MMs [4:5:6:10]		chrX:-143681805
28	AGATCGTAGGCAGAAACAAGGAG	0.8	3MMs [8:9:20]		chr17:+86085464
29	AGATACTGATCAGAAACAAATAG	0.7	4MMs [5:6:8:10]		chr18:-79273102
30	TGACTGTTAGCAGAAACAATAGG	0.7	4MMs [1:4:5:20]		chr12:+57558222

b

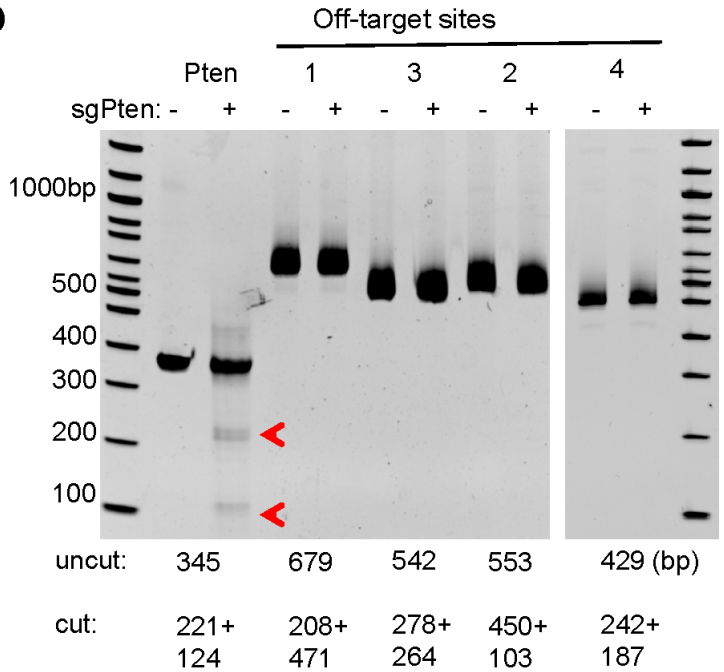

Extended Data Figure 6 | Assessing off-target cutting of sgPten. **a**, Top 30 potential off-target sites for sgPten in the mouse genome. Score is likelihood of off-target binding. Only site 4 is in the exon region of NR_045386, which is a long non-coding RNA. **b**, Surveyor assay in sgGFP (−) and sgPten (+) treated liver genomic DNA. *Pten* and *Pten* off-targets sites 1, 2, 3 and 4 were PCR amplified. Predicted size of uncut and cut bands are indicated. Red arrowheads indicate Surveyor-nuclease-cleaved *Pten* PCR products. The data are representative of two independent liver samples.

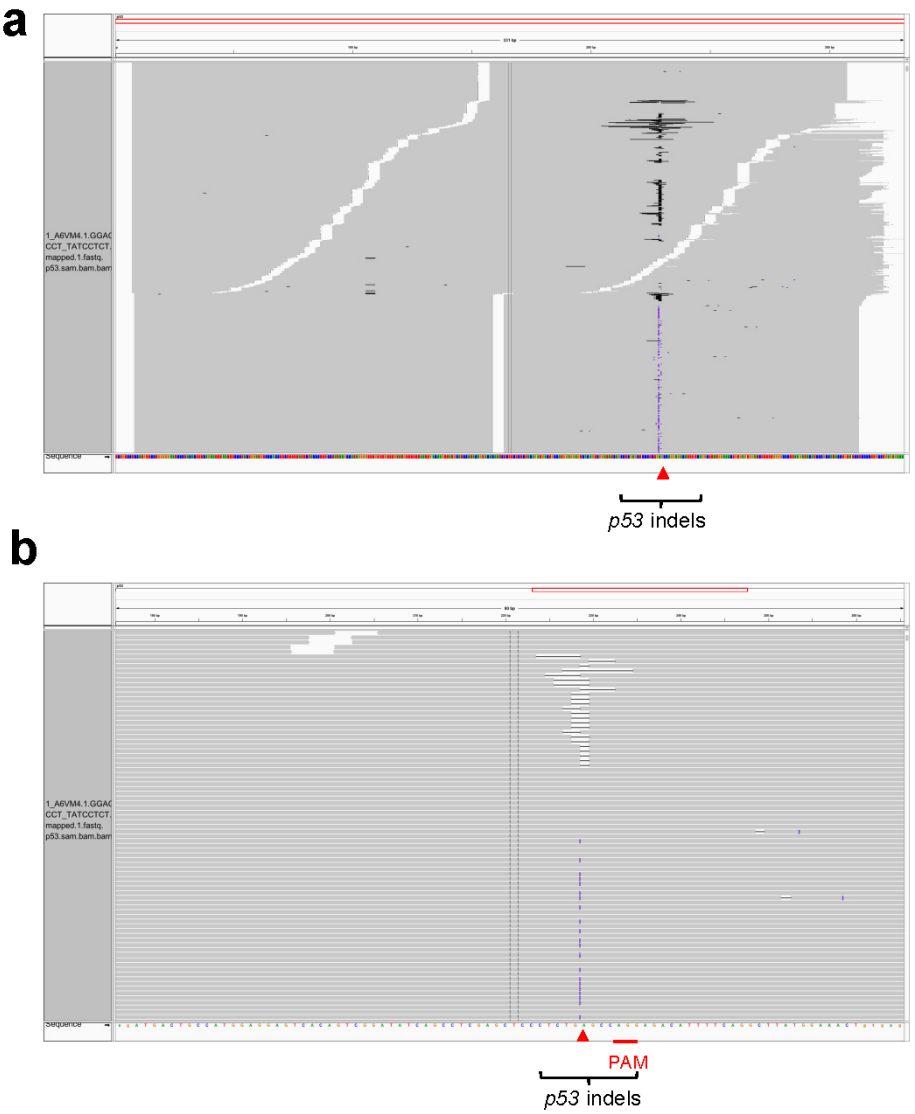

Extended Data Figure 7 | Representative *p53* indels in sgp53 treated 3T3 cells. Red arrowheads denote predicted Cas9 cutting sites. Black or purple bars in grey sequencing reads indicate deletions or insertions, respectively. **a**, p53 PCR region. **b**, Zoom in view. $n = 1$ DNA sample.

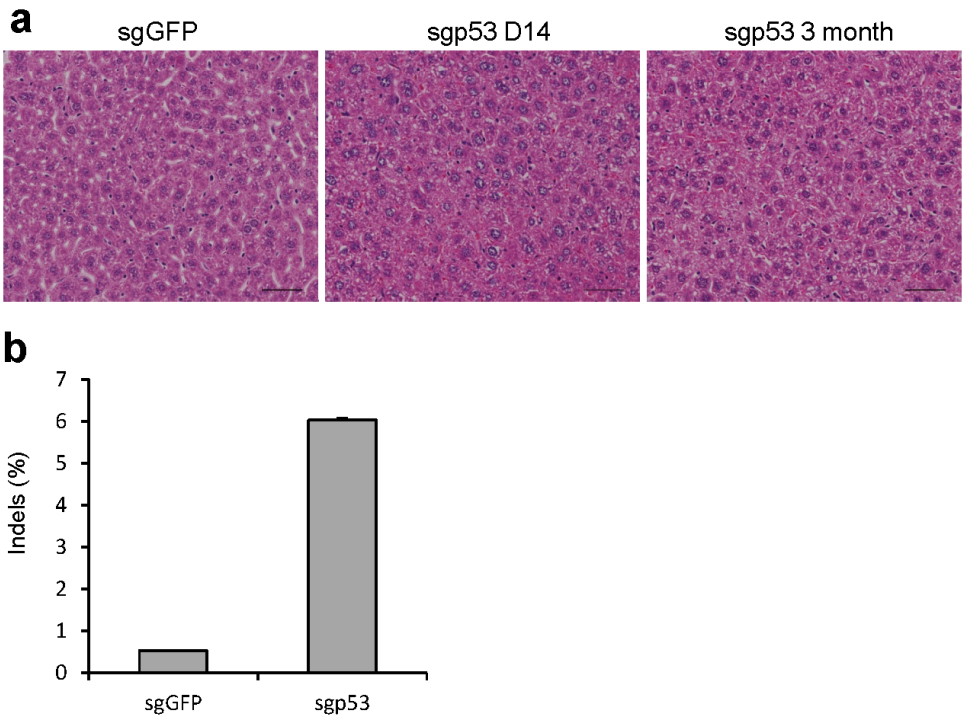

Extended Data Figure 8 | Analysing sgp53-treated livers. **a**, Histology of sgp53-treated livers. Scale bars, 50 μm, $n = 3$ mice. **b**, *p53* indel frequency was measured by MiSeq at day 14. Error bars are s.d., $n = 2$ mice.

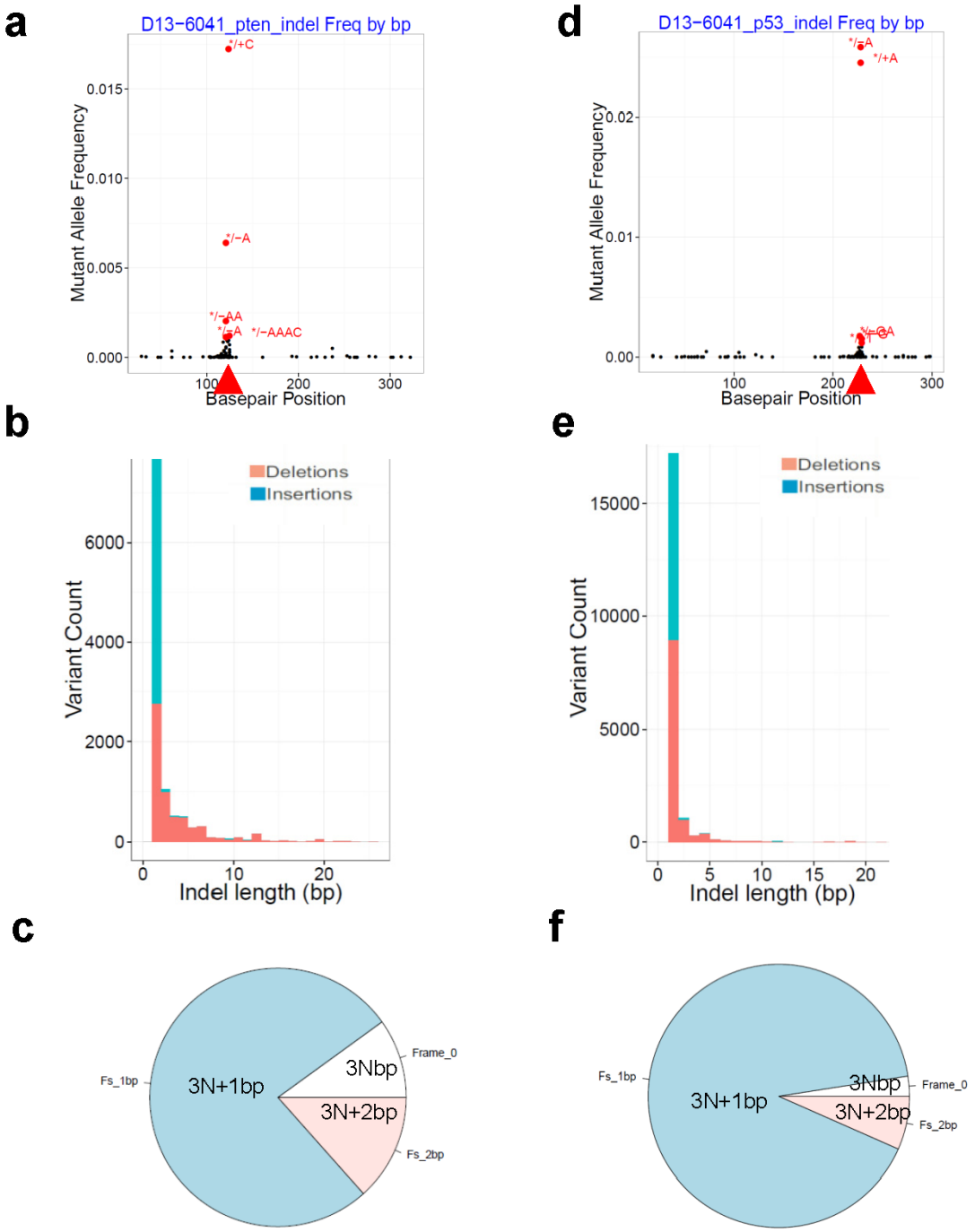

Extended Data Figure 9 | sgPten- and sgp53-generated indels in the liver. sgPten and sgp53 were co-injected into FVB mice. Representative analysis of MiSeq is shown. $n = 2$ mice. **a**–**c**, *Pten* locus. **d**–**f**, *p53* locus. **a**, **d**, Indel frequency. */+ indicates insertions and */– indicates deletions. Base pair position denotes position along the *Pten* or *p53* reference sequences. Arrowheads denote predicted Cas9 cutting sites. **b**, **e**, Distribution of indel length. **c**, **f**, Distribution of indel frame phase. Frame phase of indels was calculated as the length of indels modulus 3.

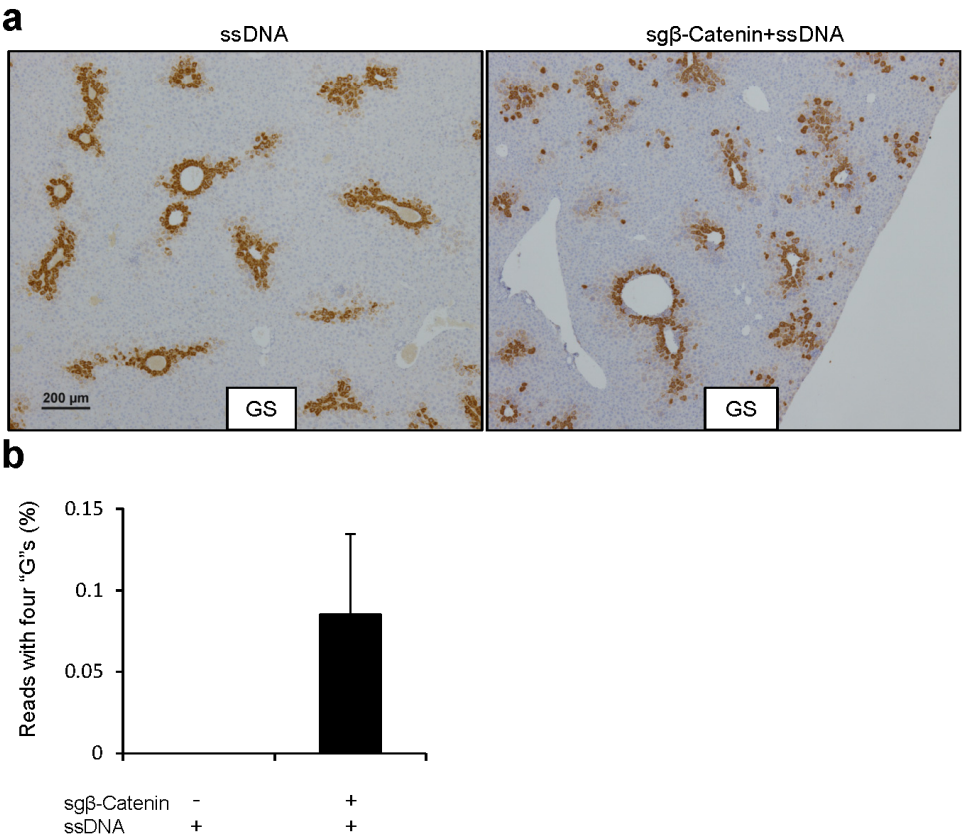

Extended Data Figure 10 | CRISPR introduces β-catenin mutations in the liver. **a**, Low-magnification images of glutamine synthetase (GS) IHC as in Fig. 4c. **b**, Frequency of *Ctnnb1* deep sequencing reads with all four G nucleotides. The rate of β-catenin donor integration was calculated as donor allele frequency. $n = 2$ mice.